A METHOD PREDICTING TEMPERATURE RISE OF OIL-HYDRAULIC SYSTEM CONSIDERING HEAT BALANCE BETWEEN OIL-PASSAGE AND HOUSING

Kouki TOMIOKA[(a)], Kazuhiro TANAKA[(b)], Hiroshi HIGO[(b)], Fumio SHIMIZU[(b)]

[(a)] NITTO DENKO Co., Ltd. Engineering Center, 18 Hirayama Nakahara-cho Toyohashi Aichi, 441-3194, Japan
[(b)] Dept. of Mechanical Information Science and Technology, Kyushu Institute Technology,
680-4 Kawazu Iizuka, Fukuoka, 820-8502, Japan

[(a)]kouki_tomioka@gg.nitto.co.jp, [(b)]kazuhiro@mse.kyutech.ac.jp,
[(c)]higo@tech-i.kyutech.ac.jp, [(d)]shimizu@mse.kyutech.ac.jp

ABSTRACT
Aircrafts have actuators as key elements such as electro-hydrostatic actuators (EHA). They are so compact and highly-pressurized. The small heat capacity or the small surface of heat dissipation for high heat load causes high temperature rise of the system. This paper summarizes the thermal modeling effort and its utility in designing a thermal predicting solution for an oil-hydraulic system. Lumped-parameter thermal models coupled with three-dimensional analysis method by CFD (Computational Fluid Dynamics) have been developed to characterize component heat transfer within their operating environments. The results on time-variant temperature rise in each component, simulated by the method, agree well with the experimental data.

Keywords: oil-hydraulic system, temperature prediction, bondgraphs, CFD

1. INTRODUCTION

An oil-hydraulic system has become smaller and highly-pressurized especially in aircrafts, where electric actuators, such as electro-hydrostatic actuators (EHA), are used for moving flight control surfaces. In the industrial field, the use of EHA is an integral part of the more-electric aircraft concept to replace inefficient centralized hydraulic systems with power-on-demand electrical systems (Navarro, 1997; Johansson, Anderson, and Krus 2001; Takebayashi and Hara 2004; Rito, Denti, and Galatolo 2010). Removing the centralized hydraulic system will, however, eliminate an effective heat transfer network, thus resulting in an aircraft with less overall heat to reject but with localized “hot spots”. Because of small heat capacity and small surface area for heat dissipation in EHA, the system is raised to high temperature while it works for long time under highly loaded condition. The high temperature rise causes deterioration of working oil and the system may become hard to control finally. From this viewpoint, it is important to study a practical way to predict precisely system temperature rise.

Energy losses cause temperature rise in an oil-hydraulic system. In this case, modeling and simulation by the bondgraphs method is effective to predict the temperature rise because the bondgraphs method is based on energy balance (Karnopp, Margoils, and Rosenberg 1975; Dransfield 1981; Thoma 1990). Some studies have been performed to predict the temperature rise of an oil-hydraulic system considering heat generation and heat transfer in components. Yamamoto, Tanaka, Nakanishi, and Tarumi (1997) analyzed heat generation and heat transfer in an oil circuit of a mobile crane by the bondgraphs method and obtained good agreement between the calculated results and the experimental results. Johansson, Anderson, and Krus (2001) analyzed heat generation from a hydraulic motor embedded in an aircraft EHA system and heat transfer from oil passages. Takebayashi and Hara (2004) and Tomioka, Tanaka, and Nagayama (2005) proposed a new idea to predict the temperature rise of a hydraulic pipe by considering heat exchange between the working oil and the pipe-housing. In their studies, lumped-parameter thermal models were developed to characterize component heat transfer within their operating environments and the bondgraphs method based on the models was applied to predict temperature rises of the working oil and the pipe-housing by coupling with three-dimensional (3D) heat conduction analysis. The time-variant temperature distributions were well predicted both in the pipe housing and in the working oil. Thermal management designed for time averaged heat load for an oil-hydraulic system is generally considered to be not adequate since those heat loads are highly transient and localized in nature. However, the studies prove reliability and effectiveness on temperature prediction using the bondgraphs simulation where the calculating time step is very small.

Then, Tanaka, Tomioka, Fuchiwaki, and Suzuki (2011) developed the above idea to predict time-variant temperature distributions in an oil-hydraulic cylinder by comparing with 3D Computational Fluid Dynamics (CFD) analysis, because the temperature distribution changed while the cylinder works for long time. The

study showed that in order to predict more precisely the temperature change inside the cylinder while the piston was moving, it was unsuitable to increase cell number merely and the optimal number of cells existed in modeling using lumped parameter modeling system. Because there were two characteristic regions inside the cylinder, one-dimensional flow pattern region like laminar flow and three-dimensional flow pattern region like turbulent flow. The latter flow pattern region should be modeled as one lumped cell.

In this study, the above-mentioned predicting methods were applied to an actual hydraulic system and the results calculated by the method were compared with the experimental data in order to validate the temperature-predicting method.

2. NOMENCLATURE

A [m^2]	heat dissipation surface area of cylinder
a [m]	representative length of inlet head port
b [m]	length from cylinder end to inlet port center
c_p [J/kgK]	specific heat at constant pressure
D [m]	cylinder diameter
E [J]	internal energy
H [J]	enthalpy
h [W/m^{2}K]	heat transfer coefficient
LoD [m]	characteristic distance of boundary between 3D and 1D flow pattern region
N [s]	reciprocating motion cycle of piston
P [Pa]	pressure
Q [m^3/s]	volumetric flow rate
R_c [m]	standard diameter of inlet head port
$\dot{q}$ [W]	amount of heat inflow
T [K]	temperature
t [s]	time
U [m/s]	velocity vector
V [m^3]	volume of cylinder head chamber
v [m/s]	velocity
W [W]	power consumed for outside
x [m]	axial location of piston head
δ [-]	Kronecker delta
λ [W/mK]	thermal conductivity
μ [Pas]	viscous coefficient
ν [m^2/s]	kinematic viscous coefficient
ρ [kg/m^3]	density

Suffix

c	cylinder
in	inflow
p	piston
$1D$	one-dimensional
$3D$	three-dimensional

3. TEMPERATURE PREDICTING METHOD IN EACH COMPONENT OF HYDRAULIC CIRCUIT

3.1. Test Experimental Circuit

Figure 1 shows a diagram of the test hydraulic circuit, which mainly consists of a pump, pipes, a control valve, a relief valve, a hydraulic cylinder, and a tank. The

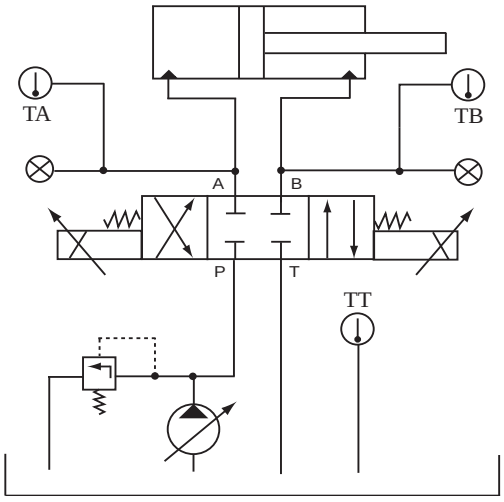

Figure 1: Oil-Hydraulic Circuit

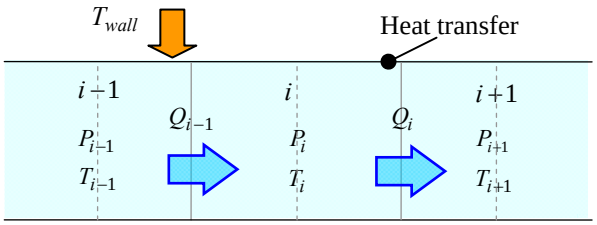

Figure 2: Pipe Model for Heat Balance

control valve is a closed center proportional solenoid valve. TA, TB, and TT indicate the temperature measurement of working oil at Port A, Port B, and the tank, respectively.

3.2. Temperature Rise Prediction in Pipe and Pipe-Housing (Tomioka, Tanaka, and Nagayama 2005)

The diagram of this heat balance type is shown in Fig. 2, where suffix i means the index of the pipe component in hand, i-1 the index of a neighboring upstream side component and i+1 the neighboring downstream side component. Temperature of each pipe component is simulated by heat balance among the heat generation in the component, the heat transfer from the pipe wall to the internal oil and heat transportation between the neighboring components of the pipe. Assuming that working oil does not work to outside of the pipe component i, rate of internal energy increase is expressed as follow.

$$\frac{dT_i^n}{dt} = \frac{1}{c_v \rho V_i}\left\{\left(P_{i-1} - P_i\right)^n Q^n + c_v \rho Q^n \left(T_{i-1} - T_i\right)^n + \dot{q}_i^n\right\} \quad (1)$$

The first term in the right-hand side indicates energy loss by pressure difference and the second term energy transferred from the upstream side component. Third term $\dot{q}$ is expressed by Eq. (2).

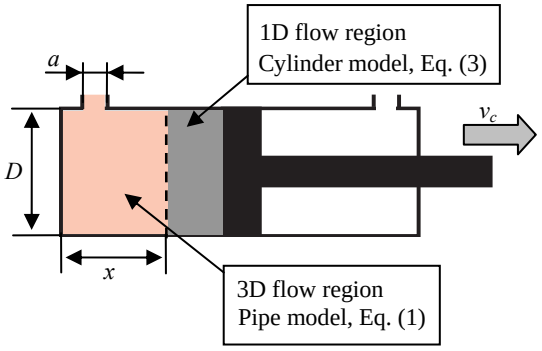

Figure 3: Heat Balance in Cylinder Head Chamber

$$\dot{q}_i^n = hA_h(T_{wall} - T_i^n) + \lambda A \frac{T_{i-1}^n - 2T_i^n + T_{i+1}^n}{2l} \quad (2)$$

The first term indicates heat amount transferred from the pipe wall to the inner working oil and the second term heat conduction between neighboring components of pipe. Heat generation and heat transfer in the pipe is calculated by Eq. (1) in each component.

3.3. Temperature Rise in Piston Head Chamber

(Tanaka, Tomioka, Fuchiwaki, and Suzuki 2011) Figure 3 shows a schematic figure of heat balance in a cylinder head chamber. Temperature in the chamber is calculated as the sum of amount of heat inflow and outflow of working oil, volumetric change of working oil, and heat dissipation to cylinder housing, which is represented by Eq. (3).

$$\frac{dT_c}{dt} = \frac{1}{c_p \rho V_c}\left\{c_p \rho Q T_i + hA_c(T_{wall} - T_c) - c_p \rho T_c \frac{dV_c}{dt}\right\} \quad (3)$$

$$if \quad Q \geq 0(in) \; T_i = T_{in}$$
$$Q \leq 0(out) \; T_i = T_c$$

In the above equation, the first term of right hand side indicates the heat flux driven by inflow or outflow with piston motion, the second the heat flux transferred between the cylinder chamber and cylinder housing, and the third the effect of cylinder volume change, respectively.

From the results by 3D CFD analysis on the flow inside the cylinder chamber during the piston movement, it was verified that the inside flow could be modeled into two patterns characteristically, one of which was 3D vortex flow pattern near the inlet port and another of which was 1D parallel flow pattern near the piston head. So, it became possible to predict precisely the temperature distribution in the cylinder head chamber preferably by incorporating the internal flow patterns with the lumped parameter models.

The dimensionless distance from the end-wall of the head chamber to the location of boundary between 3D and 1D flow pattern region was defined as *LoD*, where the representative length was *a*. Dimensional analysis was performed and derived that *LoD* was a function of the following three terms, such as the

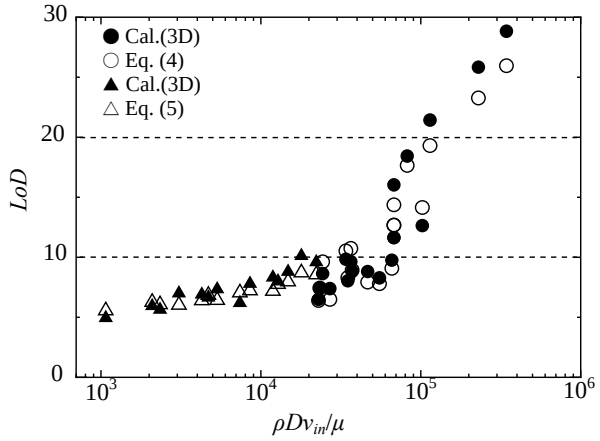

Figure 4: *LoD* with a Reynolds Number

product of the dimensionless length *D/a* and one Reynolds number expressed by $\rho Dv_p/\mu$, another Reynolds number expressed by $\rho Dv_{in}/\mu$, and another dimensionless length *b/a*.

After many simulations based on 3D CFD method, the results were obtained in Fig. 4, where the data expressed by "Cal.(3D)" were the calculated results. The abscissa and vertical axis indicate the Reynolds number expressed by $\rho Dv_{in}/\mu$ and the dimensionless length *LoD*, respectively. Figure 4 gives the line of splitting at $\rho Dv_{in}/\mu = 2.3\times10^4$ between one region with lower gradient and another region with higher gradient. By coupling this result with the above described result of dimensional analysis, the following characteristic equations were derived crossing the split line.

LoD:

(i) $\rho Dv_{in}/\mu \geq 2.3\times10^4$

$$\frac{x}{a} = 1.44\left(\frac{D}{a}\cdot\frac{\rho Dv_p}{\mu}\right)^{-0.014}\left(\frac{\rho Dv_{in}}{\mu}\right)^{0.19}\left(\frac{b}{a}\right)^{0.27} \quad (4)$$

(ii) $\rho Dv_{in}/\mu < 2.3\times10^4$

$$\frac{x}{a} = 0.015\left(\frac{D}{a}\cdot\frac{\rho Dv_p}{\mu}\right)^{-0.69}\left(\frac{\rho Dv_{in}}{\mu}\right)^{0.96}\left(\frac{b}{a}\right)^{0.098} \quad (5)$$

Figure 4 shows the comparison of *LoD* obtained through the above characteristic equations, expressed by "Eq. (4)" or "Eq. (5)", with *LoD* obtained through 3D CFD calculations. Though there is small difference less than 14%, the both results agree well. It is verified that *LoD* can be predicted suitably through the above characteristic equations.

In predicting the temperature rise in the chamber one-dimensionally, Eq. (1) is used in the 3D flow pattern region because its volume does not change and Eq. (3) is used in the 1D flow pattern region because its volume changes with time when the piston moves.

3.4. Temperature Rise in Valve and Tank

Because a hydraulic valve generates the highest pressure loss among any component in a hydraulic system, it is very important to predict heat generation there. A schematic diagram to predict temperature rise

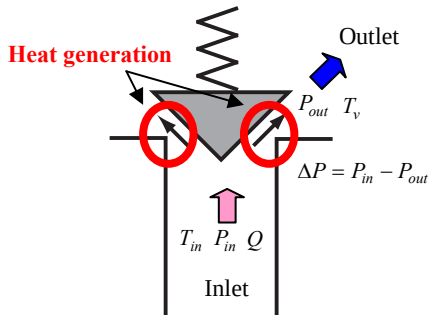

Figure 5: Valve Model

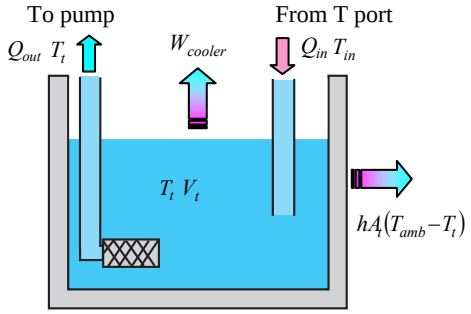

Figure 6: Tank Model

in a valve is shown in Fig. 5, which shows an example of poppet type valve. When working oil flows through throat part between the valve body and valve housing, high pressure loss appears and it changes to be heat generation.

$$\frac{dT_v}{dt} = \frac{1}{c_p \rho V_v}\left\{\Delta P Q + c_p \rho Q(T_{in} - T_v) + hA_h(T_{wall} - T_v)\right\} \quad (6)$$

A heat conduction term is neglected in Eq. (6), because the working oil velocity is fast in the valve. This equation covers the case of spool type valve.

Figure 6 shows a schematic diagram for heat balance in a tank. A volume of working oil in the tank changes time-dependently due to the sum between inflow rate from T-port of a valve and outflow rate to a hydraulic pump. Consequently, Eq. (3) with a term for time-variant volume is applicable in this case. The next equation consists of terms included in Eq. (3), heat flux flowing out, and heat release by an oil cooler.

$$\frac{dT_t}{dt} = \frac{1}{c_p \rho V_t}\left(c_p \rho Q_{in} T_{in} - c_p \rho Q_{out} T_t + hA_t(T_{amb} - T_t) + W_{cooler} - c_p \rho T_t \frac{dV_t}{dt} \right) \quad (7)$$

In this equation, the heat release from the tank wall and the oil cooler is determined by the experimental measurement.

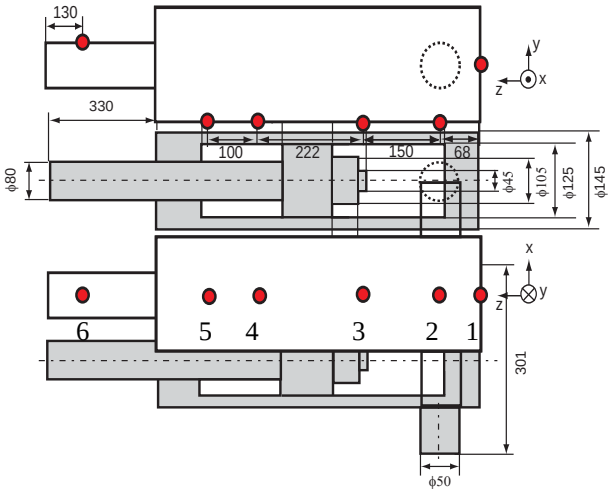

Figure 7: Schematic Figure of Test Cylinder and Measurement Points

3.5. Temperature Rise in Housings

Temperature distribution in housings can be calculated by use of a heat conduction equation, shown in Eq. (8).

$$\rho c \frac{\partial T}{\partial t} = \nabla \bullet \lambda(\nabla T) \quad (8)$$

In this study, a calculating program was made according to a finite volume method is used with Crank-Nicholson method for time-iteration. Reliability of the program was verified by comparing with the result by a commercial code, ANSYS CFX-10 (ANSYS 2005).

4. EXPERIMENTS AND CONDITIONS

The experimental measurements of temperature were conducted using the equipment shown in Fig. 1. Figure 7 shows a schematic figure of the test cylinder and measurement points in the experiment. The cylinder is a widely-used type, of which outer diameter is 145 mm and inner diameter 125 mm. In this temperature measurement test, a load for the cylinder is zero.

Temperature measurement was performed at three points in the circuit at TA, TB, and TT, which were shown in Fig. 1, and at six points on the cylinder outer surface, which were shown in Fig.7 as the number from 1 to 6.

The test conditions are shown in Table 1. In the test experiment, the temperature changes were measured when the piston was moving with constant oscillation amplitude and frequency.

Table 1: Experimental Conditions

Motion of Piston	Frequency : 0.2 Hz Amplitude : 50 mm
Supply Pressure	10 MPa
Experimental Time	1200 s
Working Fluid	ISO-VG32
Ambient Temperature	23 deg.

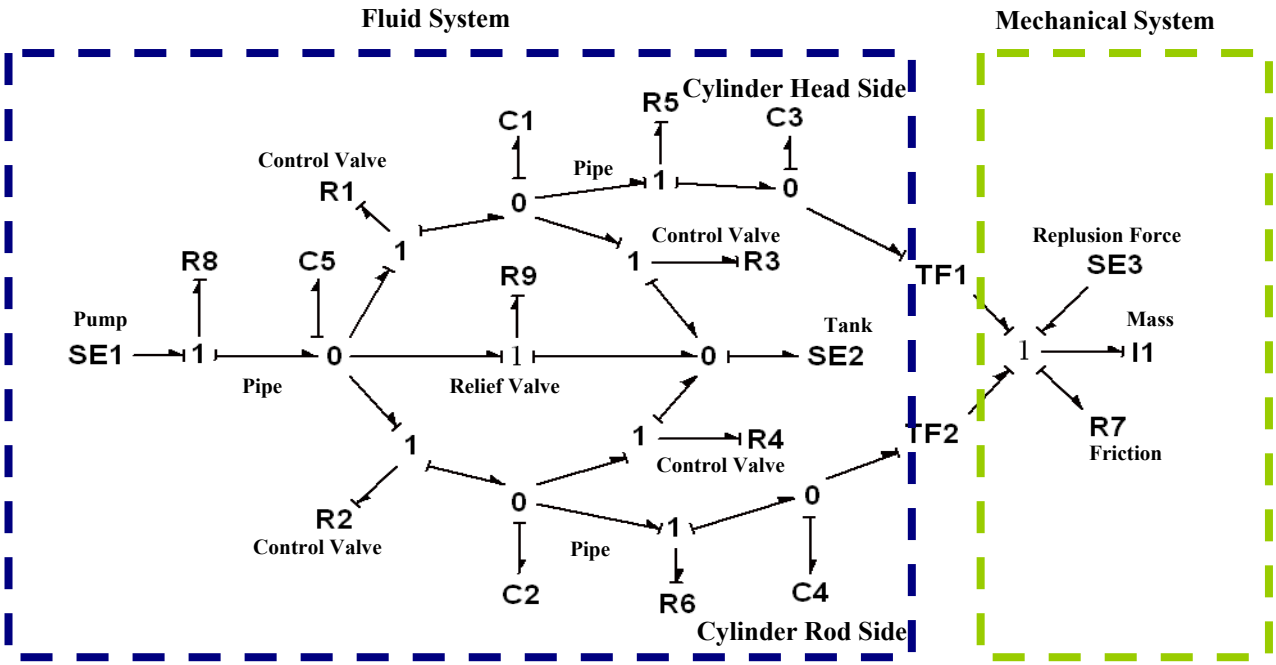

Figure 8: Bondgraph Model for Oil-Hydraulic System

5. MATHEMATICAL PREDICTION MODEL

The dynamic characteristics and temperature rise of the working oil in the system were calculated by 1D model and the temperature rise in the cylinder housing was calculated by 3D numerical method. By coupling these calculation methods, the temperature rise prediction method was established with considering dynamic characteristics of the system. This chapter shows models and parameters used in 1D modeling and simulation of dynamic characteristics and 3D numerical analysis method.

5.1. Bondgraphs model for Dynamic Characteristics

Dynamic characteristics of the working oil were analyzed by 1D modeling and simulation method using the bondgraphs. The system bondgraph correspondent to the test hydraulic system, shown in Fig.1, is shown in Fig. 8, which was introduced as a representative bondgraphs in (Dransfield 1981).

The respective element such as R1, R2, R3, and R4-element indicates resistance effect of the control valve. When the piston moves from the piston-head side to the piston-rod side, the valve-ports corresponding to R2 and R3-elements are closed and those to R1 and R4 are opened. When the piston moves in the opposite direction, the valve-ports corresponding to R2 and R3-element are opened and those to R1 and R4 are closed. The signals of valve control are given by an external program. TF-element indicates energy transfer between the fluid system and the mechanical system. C1, C2, and C5-element indicate the capacitance effect of the pipe corresponding to the respective pipe in the actual circuit. R5, R6, and R8-element indicate the pressure loss in the pipe from the control valve to the piston head

Table 2: Characteristic Equations for System Bondgraphs

Elements	Characteristic equation
SE1 (Pump)	P = Supply pressure (10 MPa)
SE2 (Tank)	P = 0.0 Pa
SE3 (Stop piston motion at the dead-end location)	$F = Repulsion\ force$
R1, R2, R3, R4, R9 (Pressure loss in Valve)	$Q = cA\sqrt{\frac{2\Delta p}{\rho}}$
R5, R6, R8 (Pressure loss in pipe)	$Q = \frac{\pi d^4}{128\mu l}\Delta P$
R7 (Friction loss between piston and cylinder)	$F = cv$
C1, C2, C5 (Capacitance effect of pipe volume)	$P = \frac{K}{V}\int Q dt$
C3 (Capacitance effect of piston head chamber; A_h=cross-section of piston head chamber, *disp.*=piston displacement)	$P = \frac{K}{V + A_h \cdot disp}\int Q dt$
C4 (Capacitance effect of piston rod chamber; A_r=cross-section of piston rod chamber)	$P = \frac{K}{V - A_r \cdot disp}\int Q dt$
TF1, TF2 (Energy transfer between fluid and mechanical system)	$F = PA$, $v = \frac{Q}{A}$
I1 (Inertial effect of piston mass)	$v = \frac{1}{m}\int F dt$

Table 3: Parameters in each element

Elements		Variables
Pipe length and diameter	R8, C5	Length = 1.0 m, Diameter = 10 mm
	C1, R5	Length = 6.0 m, Diameter = 9.5 mm
	C2, R6	Length = 5.5 m Diameter = 14 mm
Discharge coefficient	R1, R2, R3, R4	Discharge coefficient = 0.65 Valve opening area = Variable area
Valve opening area	R9	Discharge coefficient = 0.65 Valve opening area = 1.0×10^{-5} m^2
Cylinder head	C3, TF1	Length = 0.177+ *dips.* m Diameter = 0.125 m
Cylinder rod	C4, TF2	Length = 0.177- *dips.* m Head diameter = 0.125 m Rod diameter = 0.08 m
Mass of piston	I1	39 kg
Piston friction	R7	5,000 N/m
Tank surface	SE2	0.5 m^2

chamber, from the valve to the piston rod chamber, and from the pump to the control valve, respectively. C3 and C4-element indicates the capacitance effect of the cylinder head chamber and the cylinder rod chamber, respectively. SE1 and SE2 indicate the pump supplied pressure and the tank pressure. I1-element indicates the inertial effect of the piston mass and R7-element the frictional force between the piston and the cylinder. SE3-element is added as the repulsive force to stop the piston motion when the piston reaches the dead-end location of the cylinder.

Table 2 shows a list of characteristic equations used in each element. In this table, the volume of the cylinder chamber is variable because the piston displacement causes the chamber volume. Table 3 shows a list of parameters used in each element, which were measured in the test experimental apparatus.

5.2. 1D model for temperature prediction

For the temperature calculation, Eq. (3) is used in the cylinder, Eq. (1) in the pipes, Eq. (6) in the control valve, and Eq. (7) in the tank, respectively. Here, the temperature rise in the pump is not included.

A schematic diagram for 1D temperature analysis model is shown in Fig. 9, where an arrow in the figure shows heat flow direction. When the piston moves from the head side to the rod side, the heat flow calculation way is shown as follows. After the valve-ports, corresponding to R2 and R3 in Fig. 8, are closed, the working oil flows into the piston head chamber through Pipe 1, Valve 1, and Pipe 2 in Fig. 9. The heat of the inflow oil is exchanged with the cylinder housing, the temperature distribution of which is solved by 3D

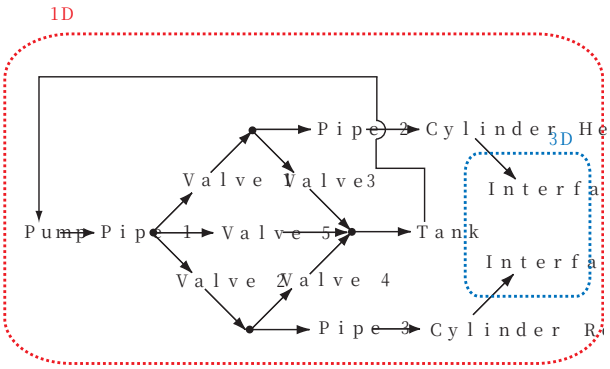

Figure 9: Heat Flow Model for Oil-Hydraulic System

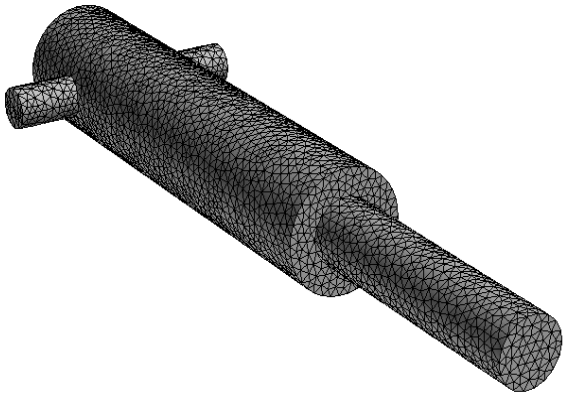

Figure 10: Numerical Grids for 3D Temperature Analysis

analysis, through Interface 1. On the other hand, the working oil in the piston rod chamber flows out after exchanging its heat with the housing through Interface 2. The outflow oil reaches the tank through Pipe 3 and Valve 4.

When the piston moves in the opposite direction, the inflow oil exchanges the heat through Interface 2 in the piston rod chamber and the outflow oil through Interface 1 in the piston head chamber, respectively. As just described, the working oil circulates in the circuit and the temperature rises at any location.

In this experiment, heat transfer coefficient was given as 10 W/m^2K from each component to the air and as 170 W/m^2K in the cooler, which was calculated reversely from the experiment.

5.3. 3D model for temperature analysis

Figure 10 shows the numerical grids for 3D calculation on temperature distributions of the cylinder. The number of numerical grid is 14000. Here, a calculating program was made according to a finite volume method and its reliability was verified by comparing with the result by ANSYS CFX-10.

Heat transfer coefficient in the cylinder head and rod chamber should be given previously before calculating heat exchange between 1D and 3D numerical analysis. Actually, because the flow rate from/to the cylinder varies with time, the heat transfer coefficient in the cylinder may also vary with time. It was difficult to determine the heat transfer coefficient

Table 4: Heat Transfer Coefficient at a *LoD*

LoD mm	h_{3D} W/m^{2}K	h_{1D} W/m^{2}K	h_r W/m^{2}K
94	118	75.4	76

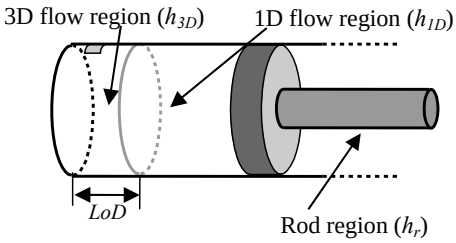

Figure 11: Definition of Heat Transfer Coefficient in Cylinder

Table 5: Analysis Conditions

Initial condition	Values measured in the experiment
Time step	3D : dt = 0.1 s, 1D : dt = 1.0×10^{-5} s
Physical property	Cylinder housing : $\rho = 7{,}850[\mathrm{kg/m^3}]$, $c_p = 465[\mathrm{J/kgK}]$, $\lambda = 43[\mathrm{W/mK}]$, Working fluid : $c_p = 1{,}900[\mathrm{J/kgK}]$, $K = 1.0\times10^{+9}[\mathrm{Pa}]$, $\lambda = 0.145[\mathrm{W/mK}]$, $\rho = 860[\mathrm{kg/m^3}]$, $\mu = 2.67\times10^{-2}\exp\{-2.9\times10^{-2}(T-40)\}$ [Pa.s], T [deg.]
Heat transfer	From housing to air : 10.0 W/m^{2}K
Ambient Air	T = 23 deg.

on the chamber inside wall, however, the coefficient was fixed to be constant in this study. Table 4 and Fig. 11 show the value of the heat transfer coefficients around the cylinder and their definitions, respectively. Table 5 shows the analysis conditions and values of the properties. Kinematic viscosity of the working oil is defined as a function of temperature.

6. RESULTS AND DISCUSSIONS

6.1. Temperature of Working Oil

Figure 12 shows the comparison on the temperature of the working oil with time at A- and B-port between in the experiment and in the calculation. In the figure, "TA" and "TB" show the A-port and B-port, respectively. "Exp." and "Cal." show the experimental data and the calculated results obtained by the proposed prediction method.

Both in the experimental and the calculated results, the temperature at A-port was higher than that at B-port. This was because A-port was connected to the cylinder head chamber and B-port the cylinder rod chamber,

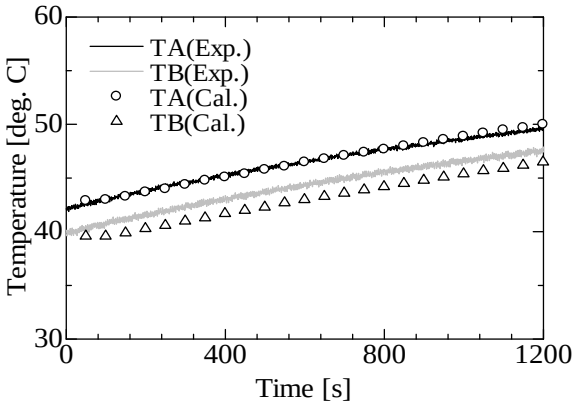

Figure 12: Temperature Change at A and B Port

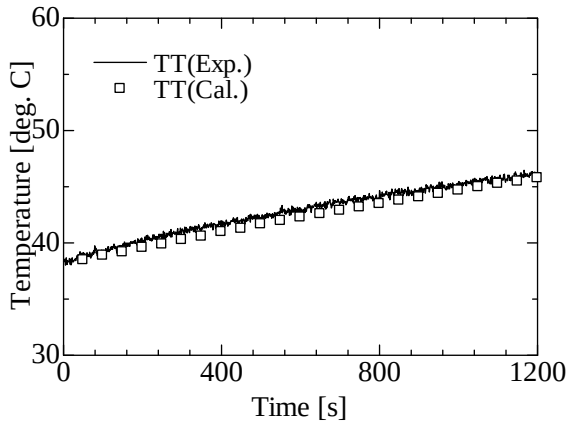

Figure 13: Temperature Change at Tank

respectively, and the cross-section of the head chamber was larger than that of the rod chamber. When the piston moved from the head to rod chamber, the flow rate into the head chamber became more than that out of the rod chamber and the pressure loss, defined in Eq. (6), became larger at A-port. In any case, the calculated results agreed well with the experimental results and the difference between both results was less than 1 deg. This fact showed that the temperature at A- and B-port behind the control valve was well predicted.

Figure 13 shows the comparison on the temperature of the working oil in the tank with time between in the experiment and in the calculation. At t= 1200 sec., the tank temperature increased up to T= 45 deg., which was lower than the temperature at A-port, T= 50 deg. This was because the volume of the tank was much larger than that of the other component. The calculated results agreed well with the experimental results and it meant that it became possible to predict precisely the tank temperature if the heat transfer coefficient from the tank could be calculated in the experiment.

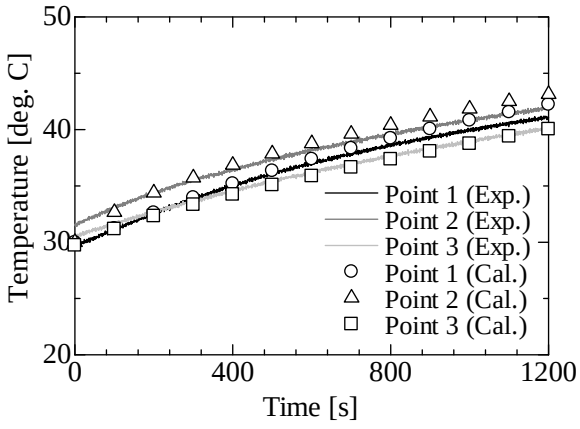

Figure 14: Temperature Change at Piston- Head Side

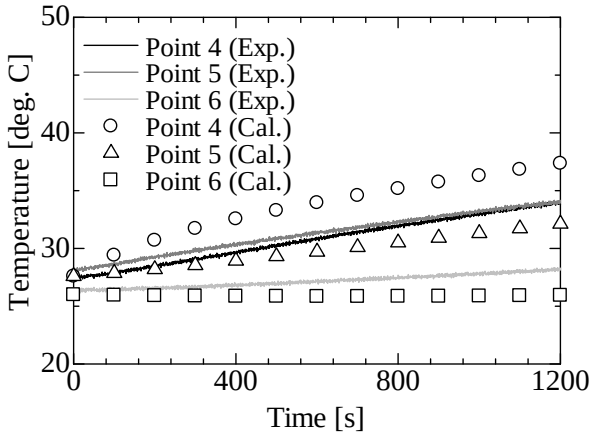

Figure 15: Temperature Change at Piston-Rod Side

6.2. Temperature of Cylinder Housing

Figure 14 shows the comparison on the temperature change at the measurement points, shown as 1, 2 and 3 in Fig. 7, on the cylinder surface in the head chamber side. The temperature increased with time at all points, because the temperature rise calculated according to 1D model was exchanged to the housing through Interface 1. The temperature at Point 2 was the highest among the three measurement points. This was because Point 2 was located just in the port inlet and the working oil with high temperature was continuously supplied there. The temperature at Point 1 was lower than that at Point2, because the wall thickness of the housing was different at Point 1, with the wall 25 mm thick, compared with that at Point 2, with the wall 10 mm thick. In any case, the calculated results agreed well with the experimental results and the difference between both results was less than 1 deg.

Figure 15 shows the comparison on the temperature change at the measurement points, shown as 4, 5 and 6 in Fig. 7, on the cylinder surface in the rod chamber side. Though the temperature at Point 4 was almost the same as that at Point 5 in the experiment, there were 5 deg. temperature differences between the two points in the calculation. One possible reason of the difference between the experimental and the calculated results might be that the contact thermal resistance between the piston rod and the cylinder, which existed actually in the experiments, was not considered in the calculation. Or, another possible reason might be that the rod chamber was modeled as one lumped parameter model because it was considered that the flow rate from/to the rod chamber was much less than that from/to the head chamber and the temperature in the rod chamber would be lower than that in the head chamber. The difference between the calculated and experimental results was less than 3 deg. at 1200 sec.

At Point 6, the temperature did not increase any more from the beginning. This was because the measurement location was far from the heat generating locations and the heat was transported merely by heat conduction in the piston rod.

Table 6: Calculation Time

Exp. Time	Calculation Time	
1200 sec.	ANSYS-CFX (Estimation)	264 days
	Proposed method PC(Power of CPU: Pentium Xeon 3.6GHz)	92 min.

6.3. Calculation time

Table 6 shows the comparison on the time for calculating temperature rise of the test hydraulic circuit between in the proposed method and in a commercial CFD code, ANSYS CFX-10. It took 92 min. for the proposed method and 264 days for the CFD code to calculate the dynamics and temperature changes of each component for the actual 1200 sec. In case of the CFD code, the time was estimated from the fact that it needed $1.9\times10^{+5}$ sec. to calculate temperature rise for 20 sec. in the actual time. The result showed that the proposed method gave very good performance.

7. CONCLUSION

In order to establish a method predicting temperature rise in an oil hydraulic system precisely and effectively, the proposed method was applied to an actual system. Dynamic characteristics of the system was analyzed by the bondgraphs and the temperature rise was calculated by 1D models, according to heat balance, coupled with 3D analysis to calculate temperature distributions in the housings. As a result, the followings become evident.

The experimental results and the calculated results on the temperature rise of the working oil were compared in the pipes, the valves and the tank, and the both results agreed well. It supported validity of the proposed method to predict temperature rise.

The calculated results on the temperature at the cylinder housing surface were compared with the experimental results. The both results agreed well at the piston head chamber side. On the other hand, there were differences between the both results at the piston rod chamber side. One possible reason of the differences might be the existence of the contact thermal resistance

between the piston rod and the cylinder or the modeling method of the piston rod chamber.

The proposed method could predict the temperature rise in an oil-hydraulic circuit effectively with the calculation time much shorter than that by a commercial CFD code.

REFERENCES

ANSYS, 2005. *ANSYS CFX-Solver, Release 10.0.*

Dransfield, P., 1981. *Hydraulic Control Systems - Design and Analysis of Their Dynamics*, Berlin Heidelberg, Germany: Springer-Verlag.

Johansson, B., Anderson, J., and Krus, P., 2001. Thermal Modeling of an Electro-Hydrostatic Actuation System. *Proceedings of the International Conference on Recent Advantages in Aerospace Actuation Systems and Components*, June 13-15, Toulouse (France).

Karnopp, D. C., Margoils, D. L., and Rosenberg, R. C., 1975. *System Dynamics: A Unified Approach,* CA: John Wiley & Sons.

Navarro, R., 1997. Performance of an Electro-Hydrostatic Actuator on the F-18 Systems Research Aircraft. NASA/TM-97-206224.

Rito, G., Denti, E., and Galatolo, R., 2010. Object-oriented modeling of flight control actuation systems for power absorption assessment. *Proceedings of the 27th International Congress of the aeronautical science (ICAS2010)*, pp.1-11. Sept. 19-24, Nice (France).

Thoma, J. U., 1990. *Simulation by Bondgraphs,* Berlin Heidelberg, Germany: Springer-Verlag.

Takebayashi, W., Hara, Y., 2004. Thermal Design Tool for EHA. *Proceedings of the International Conference on Recent Advantages in Aerospace Actuation Systems and Components*, pp.15-20. November 24-26, Toulouse (France).

Tomioka, K., Tanaka, K. and Nagayama, K., 2005. Prediction method of heat generation and heat transfer in an oil-hydraulic system. *Proceedings of Int.Conf. on Integrated Modeling and Analysis in App-lied Control and Automation (IMAACA 2005),* pp. 89-94. Marseille (France).

Tanaka, K., Tomioka, K., Fuchiwaki, M., and Suzuki, K., 2011. New Concept of Modeling to Predict Temperature in Oil Hydraulic Cylinder Chamber Considering Internal Flow. *Proceedings of Int.Conf. on Integrated Modeling and Analysis in App-lied Control and Automation (IMAACA 2011),* pp.287-292, Sept. 12-14, Roma (Italy).

Yamamoto, K., Tanaka, K., Nakanishi, M. and Tarumi S., 1997. Analysis of Dynamic Behavior of a Hydraulic and Pneumatic Suspension Including Temperature Change Effect. *Proceedings of 5th Tri. Int. Symp. on Fluid Control, Measurement and Visualization (FLUCOME97),* pp.457-462. Vol. 1. Sept. 1-4, Hayama (Japan).

AUTHORS BIOGRAPHY

Kouki TOMIOKA,

He is a chief engineer in NITTO DENKO Co., Ltd. Engineering Center. He graduated from Tanaka's Lab. In Kyuhsu Insti. of Tech. He has wide interests from engineering research and development to music concert activity. He is also a good pianist.

Kazuhiro TANAKA,

He graduated from the university of Tokyo, got the first job as an assistant professor in Sophia Univeristy, and he moved back to the university of Tokyo. After then, he moved to Kyuhsu Insti. of Tech. and is a professor. He has interests for CFD analyses on flow patterns inside oi-hydraulic valves as well as Bondgraphs.

Hiroshi HIGO,

He graduated from the graduate school in Kyushu univeristy and he is a member of research at Prof. Tanaka's lab. He has interests to analyze and control the dynamics of oil-hydraulic and pneumatic actuating systems.

Fumio SHIMIZU

He graduated from the graduate school in Tokyo university of Agriculture and Technology, and he is an assistant professor. He has interests to analyze and design for the sound propagation system.